Oriented Immobilization of Prion Protein Demonstrated *via* Precise Interfacial Nanostructure Measurements

Barbara Sanavio,[†,‡,§] Denis Scaini,[†,§] Christian Grunwald,[⊥] Giuseppe Legname,[‡,§,#,¶] Giacinto Scoles,[†,‡,#,*] and Loredana Casalis[†,§,#,*]

[†]SISSA/ELETTRA NanoInnovation Laboratory, Sincrotrone Trieste S.C.p.A., S.S.14 Km 163.5, 34149 Basovizza, Trieste, Italy, [‡]SISSA, Scuola Internazionale Superiore di Studi Avanzati, via Bonomea, 265, 34136 Trieste, Italy, [§]ELETTRA, Sincrotrone Trieste S.C.p.A., S.S. 14 Km 163.5, 34149 Basovizza, Trieste, Italy, [⊥]Johann Wolfgang Goethe-Universität, Frankfurt am Main, Institute of Biochemistry, Biocenter Max-von-Laue-Strasse 9, D-60438 Frankfurt, Germany, [¶]ELETTRA Structural Biology Laboratory, Sincrotrone Trieste S.C.p.A., S.S. 14 Km 163.5, 34149 Basovizza, Trieste, Italy, and [#]Italian Institute of Technology, SISSA Unit, Via Bonomea, 265, 34136, Italy

ABSTRACT Nanopatterning of biomolecules on functionalized surfaces offers an excellent route for ultrasensitive protein immobilization, for interaction measurements, and for the fabrication of devices such as protein nanoarrays. An improved understanding of the physics and chemistry underlying the device properties and the recognition process is necessary for performance optimization. This is especially important for the recognition and immobilization of intrinsically disordered proteins (IDPs), like the prion protein (PrP), a partial IDP, whose folding and stability may be influenced by local environment and confinement. Atomic force microscopy allows for both highly controllable nanolithography and for sensitive and accurate direct detection, *via* precise topographic measurements on ultraflat surfaces, of protein interactions in a liquid environment, thus different environmental parameters affecting the biorecognition phenomenon can be investigated *in situ*. Using nanografting, a tip-induced lithographic technique, and an affinity immobilization strategy based on two different histidine tagged antibodies, with high nM affinity for two different regions of PrP, we successfully demonstrated the immobilization of recombinant mouse PrP onto nanostructured surfaces, in *two* different orientations. Clear discrimination of the two molecular orientations was shown by differential height (*i.e.*, topographic) measurements, allowing for the estimation of binding parameters and the full characterization of the nanoscale biorecognition process. Our work opens the way to several high sensitivity diagnostic applications and, by controlling PrP orientation, allows for the investigation of unconventional interactions with partially folded proteins, and may serve as a platform for protein misfolding and refolding studies on PrP and other thermodynamically unstable, fibril forming, proteins.

KEYWORDS: nanografting · protein orientation · protein immobilization · prion protein · atomic force microscopy

The requirement to monitor tiny amounts of proteins within the smallest possible detection volumes for research and diagnostics is the main driving force for the development of novel protein detection devices. Ultrasensitive measurements of proteins can be achieved *"naturally"* through miniaturization by nanopatterning. Beyond high sensitivity, miniaturization also allows for parallelization, multiplexing, and eventually high throughput detection schemes.[1,2] Above all, however, miniaturization implies short diffusion times (that at high dilution are essential) and low sample consumption without a corresponding loss of signal-to-noise ratio. On the other hand, regardless of the sophistication of the sensor fabrication or signal readout, the detection limits of micro- and nanoscale solid-phase arrays for protein analytes still remain in the low pM to fM range,[1,3−5] well above the expected performances (attoM to zeptoM). So far, protein detectors ultimately rely on the specificity and affinity of analyte capture *via* antibodies or aptamers, with the biorecognition process being governed by thermodynamic equilibrium and suffering from time scale limitations. This becomes obvious in the typically diffusion limited reaction kinetics that may prevent the interaction to happen in practically reasonable time scales, especially at low concentrations (<fM range).[3,6] In addition, successful characterization of biorecognition crucially depends on the properties of the surface itself. The density of binding sites, their accessibility, and their lateral homogeneity, are some examples of properties that exert enormous influence on the biorecognition phenomenon, and the nanostructured interface has to be carefully engineered at the molecular level. As a consequence, an improved understanding of the physicochemical characteristics of the recognition process and the properties of nanoscale protein detection devices is necessary to push and optimize their performance, particularly for the recognition and immobilization of intrinsically disordered proteins. Their folding and stability, in fact, might be easily influenced by environmental factors and the effect of local confinement.

*Address correspondence to gscoles@princeton.edu, loredana.casalis@elettra.trieste.it.

Received for review August 2, 2010 and accepted October 13, 2010.

Published online October 19, 2010. 10.1021/nn101872w

Atomic force microscopy (AFM)-based techniques like dip pen nanolithography,[7] native protein nanolithography,[8,9] nanografting,[10] and reversal nanografting[11] have successfully demonstrated patterning of molecules, including stable and functional proteins structures, with submicrometer resolution. In addition to diverse fabrication strategies, different functionalization chemistries[12] have been reported, from covalent[11] to bioaffinity-mediated immobilizations.[8,9] Among the latter, chelator mediated his-tagged protein capture has been proved a stable and efficient way to trap proteins in uniform orientation and functional state in a pattern suitable for nanochip devices.[9] Moreover, the intrinsic versatility and subnanometer resolution of AFM provides a comprehensive tool for surface biochemical studies, for controlled nanofabrication and subsequent investigation of the interactions between the molecules and with the interface *via* both height measurements and lateral deflection (*e.g.*, molecular friction) with respect to a very flat reference substrate.

To our knowledge, very little attention has been devoted so far to the characterization of surface nanostructures of prions immobilized in a controlled orientation. On one hand, fibrillar growth has been characterized by AFM, but with little control over the orientation of the monomeric prions.[13,14] Surface-based assays like ELISA or Biacore, on the other hand, have converged toward analytical devices able to study biorecognition phenomena but without the potential sensitivity that nanoscale control of the surface functionalization implies.

The prion, PrP^{Sc}, consists of a conformationally altered isoform of the prion protein (PrP), a normal, membrane-anchored host protein, designated as PrP^{C}. Prion replication seems to involve the direct interaction between a pathogenic PrP^{Sc} template and the endogenous cellular PrP^{C}. This interaction has been proposed to drive the formation of nascent infectious prions[15] and to be at the basis of prion disorders. Prion diseases, which can manifest themselves as genetic, infectious, and sporadic disease, are probably the neurodegenerative diseases for which the largest amount of data have been collected for both humans and animals.[16] Recombinant (rec) mouse (Mo) PrP has been largely investigated in cellular systems and structural studies.[17,18] The discovery that recMoPrP residue 89 to 230 (hereafter recMoPrP(89-230)) can produce infectious prions when polymerized into amyloid fibrils *in vitro* has opened many new avenues of research[19] because it provides a platform for the study of prion replication *in vitro*. Prion studies would clearly benefit from the existence of a low protein consumption nanoscale assay, such as the present one. Potential fields of application are *in vitro* studies investigating interactions and/or related morphological changes of PrP in native-like (or physiological) conditions. While the overall goal of the present work is the development of novel routes for oriented immobilization of recMoPrP molecules on a solid surface for further morphological and biorecognition studies, one major outcome of our research is also the expected development of effective diagnostic strategies for possible early detection of prions in prion diseases. In fact, no effective *ante-mortem* diagnostics for prion diseases have been developed to date, as, among the difficulties, the infectious concentration is expected to be below the detection limit of standard techniques like ELISA and Western Blot.[1,20−22]

We show here that nanografting enables the immobilization of recMoPrP(89-230) in an oriented manner and the study of its interactions by means of carefully executed topographic measurements on a very flat surface. As a substrate, a very flat gold film covered by a monolayer of alkane-thiol supported triethyleneglycol serves as a reference which we call "the carpet". After functionalization of the substrate with one of *two* different Fabs (antigen binding fragment of antibodies) and topographic measurements in contact mode (CM) AFM in a liquid environment, we were able to detect not only the successful recognition of recMoPrP(89-230), but also the two different orientations of the PrP in the two different configurations. The differential height increase (between two subsequent steps) over the nanopatches is in good agreement with the molecular size of the immobilized protein. To this end, we compared our experimentally determined topographic heights with previously published NMR and/or crystal structures.

RESULTS AND DISCUSSION

Nanofabrication, Nanoassembly and Characterization of the Nanopatterns. Nanografting is a tip-based nanolithography in a liquid environment that exploits the force exerted by the scanning tip to facilitate the exchange of the molecules of a preexisting self-assembled monolayer (SAM) with the thiols to be patterned coming from the surrounding solution. This powerful technique introduced by Liu and co-workers[10] in 1997 has, typically, a factor of 10 better resolution than the more widely known dip pen nanolithography and has been recently successfully used in our laboratory for the monitoring of several surface biochemical reactions.[23−27] Passivating triethyleneglycol-terminated SAMs are commonly used because of their antifouling properties,[28] and here they provide the reference carpet in which metal chelating thiols (*e.g.*, nitrilotriacetic acid (NTA)-terminated thiols) can be patterned at different densities. Varying the packing density of NTA molecules that are accessible to the solution is a convenient way to tune the capture of His-tagged probe Fabs, and therefore Fab density, maintaining an overall homogeneous distribution of probes on the patch suitable for topography measurements. With nanografting, NTA packing density can be routinely varied in a reproducible manner by operating on two parameters: primarily by vary-

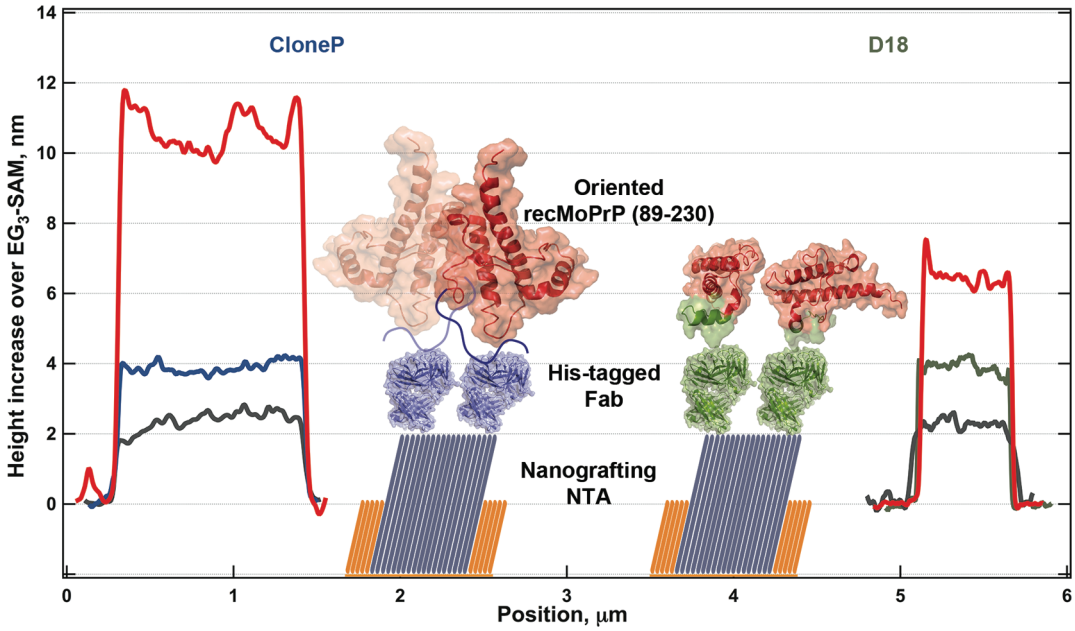

Figure 1. Cartoon of the oriented immobilization of recMoPrP(89-230) on Fab-derivatized surfaces, with average height profile resulting at each step of the assay (pH 7.4). After nanografting of NTA-EG_3-C_{16}-SH into a reference carpet of protein repellent EG_3-C_{11}-SH, histidine-tagged Fabs (CloneP, on the left, and D18, on the right) are immobilized in different experimental runs taking advantage of His-tag-Ni-NTA interaction on the nanopatches. Afterward, the sample is incubated in a solution containing recMoPrP(89-230) 300 nM. At each step of the assay, topographic measurements (CM-AFM profiles are reported here) are collected for each nanopatch. Protein models are based on previously published structures (*e.g.*, see 1hh0.pdb for Fab[33] and 1qm0.pdb for recMoPrP[34]). RecMoPrP structures are drawn at the same scale when oriented on the two different Fabs; blue tail represents the unstructured part not resolved by NMR spectra, where CloneP binds; D18 epitope is colored in green.

ing the concentration of the grafting solution, and secondarily by changing the ratio between the actual area scanned by the tip and the area of confinement (scan density ratio).[23]

Concentrations between 14 and 450 μM NTA-thiol in pure ethanol were used during nanografting in order to dose the total amount of antibody subsequently self-assembling on the nanoscale patch. Efficient substitution of the preexisting EG_3-SAM was achieved above μM concentrations of NTA. As an example, Figure 1 depicts typical results that were obtained with NTA patches nanografted at 450 μM NTA-thiol. If not otherwise stated, the scan density ratio is always 2.56 (see Methods for density ratio definition).

Metal complexes like Ni^{2+}-NTA are commonly used in affinity purification and immobilization strategies,[27,28] since they allow for reversible affinity capturing of histidine-tagged proteins in a known orientation. Previously, micro- and nanopatterning of NTA-functionalized SAMs have been exploited for oriented immobilization of targeted proteins.[8,9] Here, however, by coordination of Ni^{2+}, two different histidine tagged recombinant Fabs, D18 and Clone P, were separately immobilized at controlled density and orientation, on nanopatches, allowing for optimized and oriented immobilization of the recMoPrP(89-230), a truncated recMoPrP that largely lacks the unstructured N-terminal region. CloneP[31] and D18[32] have been extensively studied *in vivo* and also *in vitro* in their binding properties toward PrP^C and PrP^{Sc} and the recMoPrP. D18 recognizes the epitope spanning residues 132−156, that is considered important in the prion replication, while CloneP blocks a stretch of positively charged aminoacid spanning residues 95−105 in the very flexible *N*-terminal part.

Figure 1 reports an example of height profiles recorded with reference to the surrounding carpet of EG_3-thiols, and the specific height increase over the patch at each step is neatly recorded by AFM topographic measurements. Nanostructured surfaces were used to capture in controlled orientation recMoPrP(89-230) in two different buffer conditions to study the effect of pH on protein immobilization. At pH 7.4, at physiological condition, the two differently Fab functionalized surfaces were exploited as an immunoassay to capture the target recMoPrP(89-230) at different concentrations and to perform binding studies.

Topography Detection of Oriented Immobilization of recMoPrP(89-230). After nanofabrication, NTA nanopatches (varying in size from 0.5 × 0.5 μm^2, 128 lines, and 1 × 1 μm^2, 256 lines) were functionalized with the two different Fabs at pH 7.4 in TBS (Tris-buffered saline, 20 mM TRIS buffer, 150 mM NaCl), that is compatible with the reported affinity studies[31,32] on PrP both *in vitro* culture and with SPR (surface plasmon resonance). Topographic measurements using CM-AFM were conducted to discriminate the orientation of the molecules.

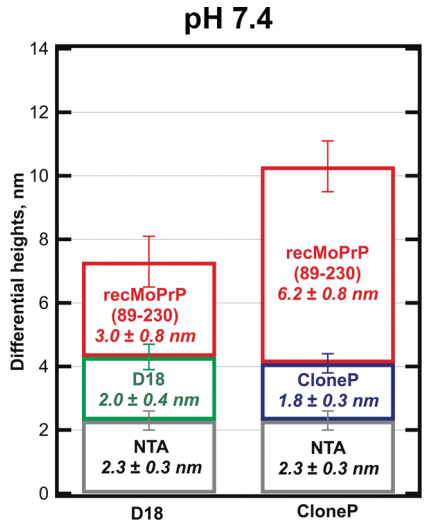

Figure 2. (a) Oriented immobilization of recMoPrP(89-230) at pH 7.4 (20 mM Tris, 150 mM NaCl) on D18 (left column) and CloneP (right column) functionalized patches. Differential height contribution relative to the NTA-thiol patch, the Fab immobilization (D18 or CloneP, respectively left and right), and recMoPrP are shown. All values are given ± standard deviation, (S.D.), as derived from two independent experiments of four nanopatches each.

NTA patches imaged in ethanol during the nanografting process showed a height increase over the carpet of 3.5 ± 0.4 nm (±standard deviation, S.D., as for other errors reported), in agreement with the theoretical difference expected from the molecule's theoretical length[35] (theoretical height difference is 3.5 nm, see Methods for calculation details).

In contrast to spontaneous self-assembly from solution, that requires a strong dilution of NTA-thiols into matrix thiols to yield ordered NTA-containing SAMs (NTA thiol could be mixed only up to 30 mol %),[36] nanografting offers a unique route to nanopatterned NTA-patches with high local concentration without compromising molecular packing and order, as demonstrated for alkanethiols.[10]

The same patches imaged right after nanografting in TBS, however, showed a height increase of 2.3 nm ±0.3 nm over the surrounding SAM (Figure 2). The carboxylic groups of the NTA moieties on the top of the supporting thiol (NTA-EG_3-$(CH_2)_{16}$-SH) are ionized, and strongly negatively charged, at pH 7.4, so that electrostatic repulsion between adjacent head groups may induce relaxation or "opening" of the NTA head groups themselves, leading to an overall lower height. This observation was confirmed by comparing the height of the patches right after fabrication in ethanol that is a less polar environment.

Once derivatized with either D18 or CloneP, the surface of the patches did show a height increase of 2.0 ± 0.4 nm for D18 and 1.8 ± 0.3 nm for CloneP, suggesting both loose packing and tilted orientation of the antibody. In fact, looking at the molecular size taken from the structure[35] of an analogue of CloneP (2hh0.pdb), the Fab would present a long major axis of about 5.6 nm, assuming that it seats straight and extended over the patch. However, if the antibody fragment was free to rotate over the blocked histidine tail, just a slight inclination of the major axis would explain a measured height of half than expected, as the vertical projection of the molecule size is now smaller. Slight differences between the measured average heights of two Fabs, CloneP and D18, may be due to both differences in the two individual structures and in the packing during self-assembly over the NTA nanopatch.

Orientation specific docking of CloneP and D18 on NTA-nanostructures was immediately evident from topographic imaging of the surface (see Figure 3). In fact, the height increase was specifically detected on the functionalized spot, and depended on the affinity between the NTA-Ni-His tag system. If the NTA surface was not loaded with Ni (II) and then challenged with Fab, no Fab immobilization was achieved (see Supporting Information, Figure S1). Moreover, the his-tagged Fab−Ni-NTA interaction was selectively displaced by highly concentrated imidazole, which competes with histidines for the binding to Ni(II) ions, as shown in Figure 3. Generally, we found that surface roughness provides an additional read out that can help with identifying different protein−surface interaction scenarios. In the case of specific interactions (see Figure 3), we found a clean EG_3-SAM with modest variation in roughness (R_q between 0.3 nm before any fabrication step, to the 0.6 nm average roughness of the surface at the end of the assay after recMoPrP immobilization). For a contaminated carpet due to unspecific protein interactions, we observed (in a few well-identifiable occasions) a significant increase in roughness (>1 nm). The roughness of the nanografted patch, that was relatively smooth at the NTA-fabrication step (on average, 0.6 ± 0.1 nm), increased as the Fab was immobilized, to 1.0 ± 0.3 nm for CloneP, while it remains constant around 0.6 ± 0.3 nm for D18.

The surfaces were challenged with a 300 nM solution of recMoPrP(89-230), a concentration high enough to ensure patch saturation. This concentration is in fact more than 100 times the known dissociation constants for both the two Fabs, thus allowing for more than 99% fractional occupancy of the binding sites. As indicated by the increase in height, the two Fabs were able to recognize their antigen. From properly oriented molecules in structure (pdb) files, obtained from previously published mouse PrP NMR data,[34,37,38] we expected an overall protein size of about 3 nm on the D18 functionalized patches, and of about 6 nm on the CloneP derivatized ones. These expectations were in very good agreement with the data shown in Figure 2. CloneP and D18 capture the recMoPrP(89-230) exposing different surfaces and different morphologies to the

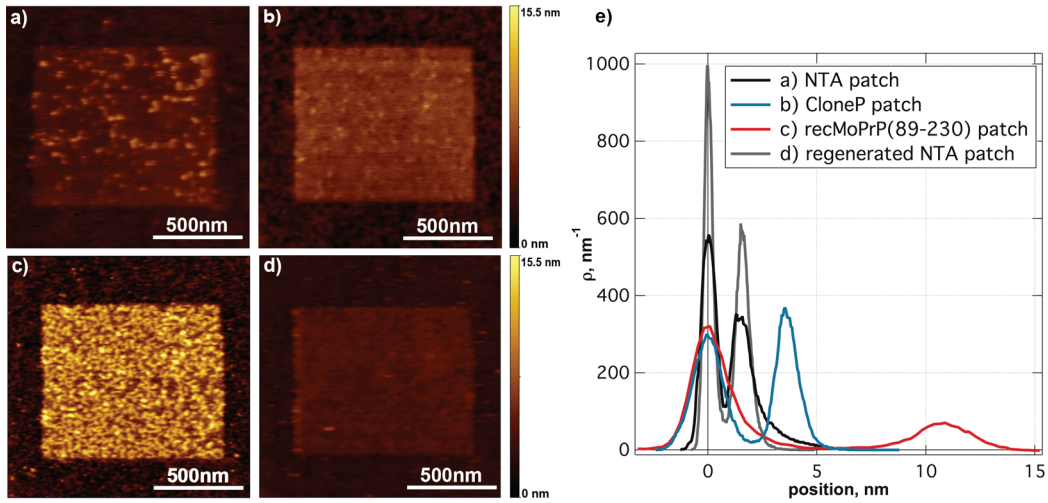

Figure 3. Topography images in TBS pH 7.4 in CM-AFM of (a) NTA nanopatterned at 1 × 1 μm², 256 lines; (b) same patch after CloneP immobilization; (c) after recMoPrP immobilization (300 nM) and (d) after surface regeneration with TBS supplemented with 400 mM imidazole, with NTA patch again ready for another round of immobilization. Color scale is adjusted to be the same in all images. Panel e shows the corresponding histogram height distributions for each image a−d (black, NTA patch after fabrication; blue, CloneP derivatized patch; red, recMoPrP(89-230) patch; gray, imidazole-regenerated NTA patch). The Gaussian peak centered at 0 corresponds to the surrounding carpet of EG_3-terminated thiols, while the second peak reveals the height distribution centered on the nanopatch, that is shifted to the right as the total height of the layer on the patch increases at each step of the assay. After thorough washing with 400 mM imidazole TBS, the NTA surface is completely regenerated (note the superimposition of the corresponding gray histogram distribution with the initially fabricated NTA patch, black curve).

AFM tip: the two distinct increases in height are due to the oriented recognition of the PrP by the Fab-functionalized nanopatches and reflect the expected molecular size of recMoPrP, as 6.2 ± 0.8 nm over the CloneP-nanopatch and 3.0 ± 0.8 nm over the D18 functionalized structures. To further confirm the extrapolated size with experimental data, another immobilization chemistry was tested. RecMoPrP(89-230) was covalently linked to nanografted patches of carboxylic-acid-terminated thiols (HS-C_{15}-COOH), activated to react with free amine groups of lysine side chains on the protein surface, giving a height of about 4 nm, but with a rough and inhomogeneous surface. The roughness was further enhanced by binding of D18 because, in this case, the protein does not present all the binding sites oriented in the same way, so not all of them are available for recognition by the corresponding antibody (see Supporting Information, Figure S2).

Antibody/recMoPrP(89-230) Recognition as a Function of Protein Concentration: Apparent Binding Constant Measurements. ***Primary Results.*** Biorecognition efficiency of recMoPrP on the two functionalized nanostructured interfaces was investigated through the estimation of apparent affinity constant (as apparent dissociation constant, $K_{d,app}$), after titration as a function of recMoPrP concentration. SPR affinity data were already reported in the literature[31,32] for measurements at pH 7.4, the same condition we chose, and these data can be used to compare how nanofabrication and surface assembly may affect the immunoassay performance. CloneP-functionalized surfaces were titrated against recMoPrP(89-230) concentrations ranging from 3 pM to 300 nM, and the average differential height increase due to deposition of the PrP molecules on the Fab functionalized patches was monitored. Differential height increase is related to specific binding onto the nanostructure and, of course, it increases as a function of the specific coverage on the spot. The height response (Δh) of recMoPrP was used to estimate an apparent affinity parameter (see Figure 4), and the roughness sig-

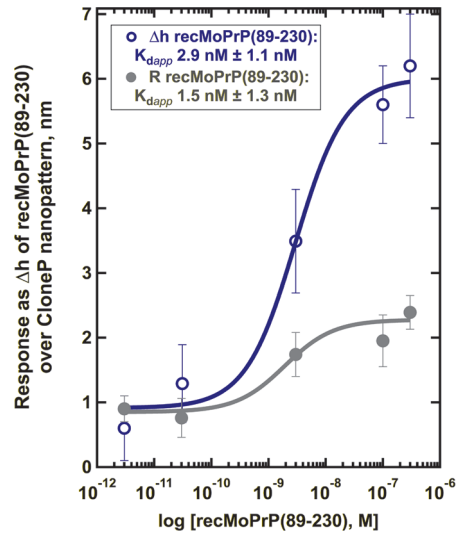

Figure 4. Dose−response curve of differential height (Δh recMoPrP, blue curve and open blue circle) contribution due to recMoPrP(89-230) binding on CloneP patches. A similar sigmoidal response is recognized from the roughness of the patch as a function of recMoPrP concentration (gray line, solid circle).

nal was used as well to further confirm the trend of specific binding on the patches.

The derived apparent affinity ($K_{d,app}$) of the molecule for he functionalized surface, that we measure to be 3 ± 1 nM (1.5 ± 1.3 nM from the roughness signal), equals or is up to 10 times larger than the estimated CloneP affinities for cognate epitope measured on macroscopic surfaces which ranges between 0.3 (hybrid mouse and bovine engineered protein), 0.5 nM (bovine peptide spanning residues 95−145), and 2.6 nM (Human peptide 95−145), as previous SPR characterizations reported.[30] At a concentration of target equal to the K_d concentration, let us say 0.5 nM recMoPrP concentration in this case, on average half of the Fab molecule would be complexed; that is, half saturation is reached and the response signal is proportionally decreased compared to the (almost) fully saturated one. We expect that, in addition to experimental error, the probably closer packing of the molecules induces the steric hindrance that is responsible for the deviation from the bulk surface value.[39,40] Indeed the roughness signal, in our case connected to the coverage on the nanopatch surface, correlates slightly better with the results obtained on extended surfaces employing SAMs. We may argue, though, that SPR data, fast and useful on large scale studies, have actually little control over molecule orientation, and many reports[1,3,39,40] highlighted how this effect is actually underestimated in surface studies. Moreover, the data we are referring to, while providing very useful comparison for our novel assay, were obtained from surfaces functionalized in the opposite way: recMoPrP or shorter peptides were chemically linked on the surface, without any preferential orientation of the binding sites toward the Fab, that was added to the solution.

The same experiment was conducted on D18-functionalized patches, but in this configuration the shorter molecular size is offered as a signature of the recognition, and at low patch saturation the average differential height increase signal is too low to be detected with sufficient accuracy, in contact mode. At 3 nM recMoPrP, the increase in height registered by us on the patch is only of 1.5 ± 0.8 nm. On the basis of the affinity reported in the literature[32] (K_d, 1.6 nM), we speculate that already in the low subnanomolar range the coverage is too loose to produce a reasonable signal. In fact, the Δh measured at 3 nM ($2 \times K_d$) is half of the signal at 300 nM concentration, which is not very far from saturation. This implies that, in this configuration, at very low concentration, the PrP coverage could not be enough to generate a sufficiently high topographic signal.

Effect of Changing the Surface Coverage of the NTA Groups. Since the density of D18 and CloneP probes was expected to play a role in the biorecognition of recMoPrP, the NTA-patch nanofabrication was varied in the 14−450 μM range of grafting concentration, and the scan density was equal to 1.28 (half than the density used in the experiment above). After fabrication topographic height and roughness measurements were performed in both contact and noncontact mode (NC). We expected NC-AFM measurements to be much less perturbative on immobilized protein, since, at low coverage, proteins may be more prone to tip-induced deformation. A test on a different buffer solution suitable for multiple pH measurements and compatible with protein immobilization was performed. Among the buffer solutions capable of covering a wider range of pH, a phosphate buffer 50 mM 150 mM NaCl was chosen. Moving from neutral (7.4) to basic (8.0) pH for imaging purposes, the height of the NTA-nanopatch at equal fabrication parameters (density of lines and grafting concentration) decreased, confirming the trend of electrostatic repulsion between head groups of the molecules. When functionalizing the NTA nanopatch with CloneP in phosphate buffer pH 7.4, noncontact (NC) measurements in liquid revealed a negligible increase in height, pointing to an extremely low density of probe. However, when titrating the surface with increasing concentration of recMoPrP (89-230), specific immobilization was achieved only on the patches, and the differential increase in height over the patch due to recMoPrP immobilization was following a sigmoidal trend, with an apparent affinity constant of 2.0 ± 0.8 and 1.6 ± 0.8 nM on patch fabricated at 450 μM and 143 μM NTA-thiol concentration, respectively (see Figure 5, panel a). At higher titer of CloneP (625 nM against the usual 300 nM) an increase of 1.2 nm was detected (on 450 μM NTA-patches), but negligible recogniton of recMoPrP(89-230) was achieved between 300 pM and 35 nM.

D18 was tested in the same condition (Figure 5b). Despite a negligible signal of D18 functionalization, patches were responding specifically to increasing concentration of recMoPrP(89-230). Saturation of the nanopatches was not achieved below nanomolar concentration, which confirmed contact mode measurements, and an apparent K_d estimation at 450 μM and 90 μM NTA patch fabrication was pointing to 2.9 ± 1.4 and 1.9 ± 1.3 nM, respectively, near the SPR data[32] (1.6 nM).

CONCLUSIONS AND OUTLOOKS

We demonstrated the oriented immobilization of recPrP molecule at the nanoscale and the measurement of the effect of confinement on biorecognition combining nanografting, bioaffinity immobilization, and differential height measurements using an AFM-based platform. Nanografting has been used previously[10,11,23−27] to study the effect of patterning of protein on the surface in different configurations, but with very little attention on the performance of the bound macromolecules in a recognition-based assay. The specific receptor protein orientation has to be homogeneous, the surface roughness should not mask

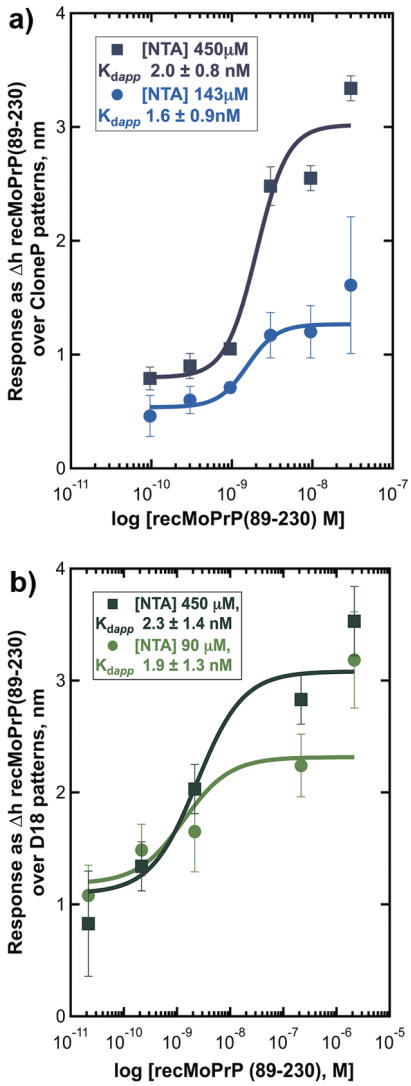

Figure 5. Dose−response curve of differential height measured in NC mode (Δ*h* recMoPrP, blue curve and open blue circle) contribution due to recMoPrP (89-230) binding on CloneP patches (panel a) and D18 patches (panel b) as a function of NTA-thiol grafting concentration (scan density equal to 1.28, imaging buffer 50 mM phosphate buffer, 150 mM NaCl, pH 7.4). The estimated $K_{d,app}$ decreases as the grafting concentration—and in turn, Fab density—decreases. However, especially for D18 functionalized patches, good S/N (signal-to-noise) ratios are achieved for NTA thiol concentration above 90 μM.

or affect the binding site accessibility from the solution, and the incubation times have to be sufficiently long to approach equilibrium and to be chosen according to the characteristic kinetic constants of the molecule under investigation. In this way the performance of the nanostructured surface can be tested in a quasi-quantitative assay. Nanografting of NTA-terminated thiol provides a very general route for specific protein immobilization in a controlled orientation, since the polyhistidine tag can be genetically engineered in recombinant protein in a known position, and the interaction with Ni-NTA complex is specific. Moreover, this immobilization is reversible and ensures reusability of the surface. The nanografted NTA-Ni-His-tag system on a flat protein repellent reference carpet generates an homogeneous surface in which the His-tagged fragment of antibodies are immobilized to maximize the distribution of the binding sites toward the solution containing the target protein. Choosing Fabs like D18 and CloneP allowed for the orientation of recMoPrP(89-230), since their binding sites are on different locations on the PrP surface. The two different configurations (CloneP immobilized recMoPrP(89-230) and D18-immobilized recMoPrP(89-230)) are discriminated by accurate measurements of the molecular size of the protein.

The minimum signal detectable from recMoPrP(89-230) binding was in the tens of picomolar, a value that depends less on diffusion-limited kinetics than on the affinity constant of the antibody; the latter being in the subnanomolar range does not allow for saturation of the nanostructure in the low picomolar range. We expect that a highly controllable surface with specific protein orientation would be very useful in the reliable testing of recognition and binding between biomolecules. Even though infectious prion concentration in peripheral blood and tissue is reported to be in the low fM range, successful detection with subnanomolar affinity antibodies could still be possible after proper sample treatment, like protein misfolding ciclic amplification (PMCA),[42] or a specific sample increased concentration that, combined with the low volume consumption of this assay, would circumvent diffusion and affinity limits of the system. Finally we would like to note that our AFM-based tools have still an enormous potential, as we can speculate that converging efforts on parallel functionalization, diffusion enhancing system, centrifugal molecule focusing, high affinity antibody, and last but not least tethered double binding molecules could further lower detection limits. A practical and lower cost version of our device will rest instead on the application of an easier to multiplex electrical readout system.

In addition to possible diagnostics applications, the strict control over PrP orientation opens many avenues of investigation of possible interacting partners, from large macromolecular complexes to small organic dyes that interact unconventionally with unfolded proteins,[43] and may serve as a platform for protein misfolding studies on PrP and other thermodynamically unstable proteins. In particular, this oriented nanoconfinement of PrP, whether in its truncated or full length from, can be used for *in situ* fibrillation studies, in which the early stage of aggregation can be followed in real time with high sensitivity as a function of multiple variables in a highly controllable environment. The use of antibodies that mask different regions of the PrP offers the advantage of understanding the assembly and interaction of proteins during fibrillation by varying the exposed region of the protein available for protein interaction. Other unstructured proteins, like α-synuclein,

β-amyloid peptide, and hungtintin,[44] offer intriguing examples to test how the nanoconfinement can provide a useful, highly controllable environment for misfolding and aggregation studies on surfaces.

METHODS

Materials and Instrumentation. EG_3-thiols (HS-$(CH_2)_{11}$-EG_3−OH, 2-{2-[2-(1-mercaptoundec-11-yloxy)-ethoxy]-ethoxy}-ethanol) were purchased from Prochimia Surfaces (Poland), NTA-EG_3-C_{16}-SH (2-{2-[2-(1-mercaptohexadec-16-yloxy)-ethoxy]-ethoxy}-ethoxy nitrilotriacetic acid) was kindly provided by Jacob Piehler. NaCl, imidazole, EDTA, $NiCl_2$, TRIS, sodium phosphate dibasic, potassium phosphate monobasic, and ethanol (99.8% purity) were all provided by Fluka and Sigma Aldrich, (Milan, Italy). All the solutions were prepared in ultrapure 18.2 MΩ · cm water (Milli-Q, Millipore SpA, Milan, Italy), and filtered with a sterile syringe-filter (0.22 μm) immediately prior to use. All other reagents were of analytical grade. All AFM experiments were carried out with conventional AFMs using a XE-100 (Park System, former PSIA, Korea) working in contact mode; Noncontact mode measurements in liquid were performed on a MFP3D Stand Alone AFM, (Asylum Reasearch, Santa Barbara, CA). For nanografting and NC-AFM imaging, commercially available silicon cantilevers (NSC19, MikroMasch, Poland, nominal spring constant 0.6 nN/nm, tip radius <10 nm) were chosen. For CM-AFM imaging purposes, a soft cantilever (CSC38B, MikroMasch, Poland, nominal spring constant, 0.03 nN/nm, tip radius < 10 nm) was used.

Protein Production and Purification. The Fabs, D18 and CloneP, were produced as previously reported with a $(HisGly)_6$ tag.[31,33] The recMoPrP(89-230) was produced and purified as reported previously.[13] All the protein stocks were kept on ice if needed and diluted immediately prior to use.

Substrate and Monolayer Preparation. Ultraflat gold film substrates were prepared using a modified Ulman procedure.[45−47] Briefly, freshly cleaved mica sheets (clear ruby muscovite, Goodfellow Cambridge Limited, Huntingdon, England) were mounted in an electron beam gold evaporator and gold films were deposited at a rate of ∼0.1 nm/s and a chamber pressure of about 10^{-6} mbar until a thickness of 100 nm was reached. A small amount of SU8-100 (MicroChem Corp., MA) polymer were then equally dropped on the gold side of the gold-mica sheet, and the polymer was then cured (baked 5 h at 95 °C, exposed 20 min under a 70 μW/cm^2, 462 nm UV lamp, and baked at least hours at 95 °C to form a sample for contact mode measurements). With a similar approach, gold was evaporated on silicon wafers (University Wafers, MA). Then, cleaned silicon slides of 5 × 5 mm^2 were glued to the gold surface using a small amount of SU8-100, that was cured a few hours at 135 °C. The SU8-drop, now looking as a flat hard surface strongly attached to the gold layer, can in this way be mechanically detached in air from the mica substrate, keeping the gold film attached to it and exposing now the gold surface originally buried at the interface with the mica. Such an Au film surface has the advantage of reproducing the flatness of mica, giving an extremely reduced roughness of about 4 Å (even when evaporated on silicon). Samples are, immediately after stripping, soaked in a freshly prepared 300 μM solution of EG_3-thiol in ethanol. The substrates were kept in the thiol solution overnight in the dark at room temperature. In this way an ultraflat surface covered with EG_3-terminated thiols was obtained. AFM test measurements confirmed a roughness in the range of 3−4 Å.

The Nanofabrication Process. In all the experiments the process of nanografting was performed in the following steps. (a) A freshly prepared SAM substrate was mounted in a closed liquid cell. Prior to grafting a worn out cantilever was used to scratch a sign into the gold surface, that allows the optical alignment of the cantilever to a coordinate system which facilitates finding back the nanopatches. (b) The liquid cell was filled with the nanografting solution (*e.g.*, a 450 μM NTA-thiol HS-$(CH_2)_{16}$-EG_3-NTA) solution. The SAM was imaged in liquid at low load to select the area where to fabricate the nanostructures. (c) The desired patches were obtained within the SAM by scanning the AFM tip above a threshold of about 70 nN, with a scan rate of 2 Hz. In this way the alkylthiol SAM phase was locally disrupted and immediately exchanged with the NTA-thiol monolayer phase. Varying the number of lines scanned by the tip during the nanografting patterning varies the actual area scanned by the tip (and where the substitution takes place): the area effectively substituted is estimated as the ratio between the area scanned (given by the contact area of the tip, 10 nm, by the number of scanned lines) and the image area: R_{tip} · lines/area. The best homogeneous NTA-patches were produced with a patch size of 500 × 500 nm^2 (*i.e.*, 128 lines S/A 2.56) or 1 × 1 μm^2, (256 lines, S/A 2.56), and a scan rate of 2 Hz. (d) After the grafting procedure, the patches were imaged in ethanol and afterward in buffer (with a soft cantilever and at low forces, namely <0.3 nN) in order to record topographic, for example, height, data. The size of the patches was chosen to be between 0.25 and 1 μm^2. According to Sheean *et al.*[6] a smaller patch size enhances the mass transport limits of the system, requiring too much time to saturate with the target the functionalized patch at low concentration (the average time is of tens of hours at fM concentration for a 1 μm^2 patch). It has been reported[46] that for a yes/no determination of target mass transport limit is not an issue, since device stability can reduce the incubation time to the minimum time required to immobilize the minimum number of molecules sufficient to give a detectable signal. However, quantification and binding characterization, which are our main concern, still depend on the average equilibration time.

Pattern Functionalization. After the nanofabrication process the surface was thoroughly rinsed with ethanol and dried. The sample was first washed with a 0.5 M EDTA (ethylenediaminetetraacetic acid, pH 8.6, Fluka) solution in order to remove undesired metal ions, with three washing steps of 4 min each, and a solution containing 10 mM $NiCl_2$ (Fluka) in 20 mM TRIS, pH 7.4 (Fluka), was loaded on the sample for 5 min. The surface was then ready for the immobilization of the histidine-tagged Fab, CloneP or D18, able to recognize the recMoPrP(89-230). The Fab was added into the AFM liquid cell as a 300 nM solution in 20 mM TRIS 150 mM NaCl (Fluka) buffer (pH 7.4) for 20 min. Height measurements revealed the presence of higher patches on the surrounding surface. No Fabs immobilization was achieved if the NTA surface was not loaded with Ni(II) (see Supporting Information, Figure S1).

Once the surface was functionalized and characterized, it was incubated at room temperature in a solution containing recMoPrP(89-230) at 300 nM concentration for 30 min. The presence of the molecule was then ascertained through height measurements after rinsing the surface in buffer.

Regeneration of the surface (removal of the PrP and the Fab) was achieved by copiously washing the surface with a solution of 0.4 M imidazole (Fluka) in 20 mM Tris buffer, and a subsequent washing step with EDTA 0.5 M was performed. The surface was then ready for another cycle of immobilization and assay measurements. Regeneration of the surface through denaturation of the interaction between the Fabs and the recMoPrP, with either low pH (pH 4) or denaturant (4 M urea) treatment, was abandoned since it was damaging the surrounding EG_3-carpet.

In the case of covalent immobilization of recMoPrP, HS-C_{15}-COOH, 100 μM was nanografted into EG_3-thiol. Then, the surface was activated for 15 min in a solution containing 5 mM DCC (*N,N′*-dicyclohexylcarbodiimide) and 15 mM NHS (*N*-hydroxysuccinimide) in Tris buffer, 20 mM, pH 7.4, and then incubated for 50 min with a 216 nM solution of recMoPrP (89-230) or a 30 nM solution (see Supporting Information, Figure S2).

Binding Studies. Different concentrations of recMoPrP(89-230) above and below the K_d (0.5 nM) of each antibody were tested, and the differential height was used as the response signal and fitted to a three parameter sigmoidal dose response equation in Igor Pro (Wavemetrics, Inc.) through Visual Enzymics 2010 (Softzymics, Inc., NJ). Tables with fit results are included in the Supporting Information. The topographic measurements were

performed after an incubation in the recMoPrP(89-230) solution long enough to reach equilibrium. The incubation time was estimated from the kinetic parameters evaluated by Safar *et al.*[31] *via* Biacore experiment: the average mean time ($1/k_{off}$) of the complex is supposed to range between half and 19 h (for the 2.6 and the 0.3nM K_d), while the average lifetime (ln ($2/k_{off}$)) spans accordingly between 0.5 and 13 h. However, considering the report of Kusnezow and co-workers,[3] we may estimate in ideal condition (absence of mass transport phenomena and steric hindrance of binding site) that the ideal time as a function of target concentration ($1/(k_{off} + k_{on} \cdot [target])$)[3] for signal "development", that is the approaching of the thermodynamic equilibrium, is shorter: from 4 s at 900 nM recMoPrP to 12 min at 300 nM, 1 h at 3 nM, and 5.6 h at 95 pM concentration. We doubled the theoretical incubation time while performing the experiment to take into account eventual deviation from ideality. Heterogeneous phase microarrays are modeled as two-compartment model systems,[3,6] since the presence of a solid phase support affects the diffusion constraints of an ideal bimolecular reaction in solution. If initially the reaction is governed by the kinetic rate constant of the specific macromolecular pair involved, then it becomes progressively limited by the diffusion rate of the target analyte from the bulk solution to the reaction spot. Even in the steady state condition, the prolongation of the estimation time actually is not dramatic, due to the small patch size compared to that of standard microarray systems.[3] Assuming the receptor molecule as a square of 4×4 nm^2, and therefore that the density of receptor ρ on a 1×1 μm^2 patch is 10^{-11} moles $\cdot$ cm^{-2}, and assuming a slow diffusion coefficient for the recMoPrP of 10^{-10} cm^2 s^{-1}, the Damkoehler number can be roughly estimated ($\rho \cdot \pi \cdot R \cdot k_{on}/(4D)$ for a circular spot[3]) and used to correct with a proportional factor the ideal time (the time needed to reach the steady state between the bulk solution and the compartment surrounding our patch, that is in our case negligible). The reaction duration actually benefits from the small size of the patches, small enough not to deplete significantly the target analyte in the reaction site. However, if higher affinity constant antibodies were used, that would have terribly affected the performance of the assay: an increase in affinity of 2 orders of magnitude (let us say, in the 20 pM range), usually related to an equivalent increase in the off rate reaction constant, k_{off}, can actually raise the ideal reaction time to more than 60 h at pM analyte concentration without any stirring or analyte concentration device.

Image Analysis. Each experiment involves the fabrication of multiple patches that contribute to the single experiment statistic, and to the interexperiments statistics. All height measurements are reported with their standard deviations. Topographic images of the patches are then analyzed in term of pixel distribution (region analysis) in order to get the height value related to the patch at each single step of the experiment (nanografting, Fab functionalization, recMoPrP loading, regeneration step). The AFM instrument proprietary software (XEI, Park System, and MFP3D, Asylum Research) and free open source software, Gwyddion (www.gwyddion.net), were used. The experimental value was then compared to the global size of the molecule as obtained from pdb files (1hh0.pdb, for Fabs, 1ag2.pdb, 1qm0.pdb for recMoPrP(89-230), visualized with PyMol, Schrödinger, LLC., http://www.pymol.org). The height of the patches is the relative height increase due to the nanostructure compared to the surrounding reference surface (SAM). Then, this height increase can be related to the fabrication and the recognition events that take place on the sensor surface as a differential height measurement. For example, the NTA patches are 2.3 ± 0.3 nm taller than the surrounding SAM (compatible with theoretical height: from the CRC Handbook of Chemistry and Physics;[35] the bond length values were computed and corrected by the bond angles between Au−S−C and C−C−C of 109.5° and by the tilting of 30° of thiols in the self-assembled monolayer: a 3.5 nm difference). After the immobilization of the Fab, the patches were 4.1 nm higher than the reference carpet. This relative height increase is due to the contribution of both the NTA-thiols (2.3 nm) and the Fab ($4.1 - 2.3$ nm $= 1.8$ nm). Error was propagated as a geometric sum.

Acknowledgment. The authors thank CBM S.r.l.—Cluster in Molecular Biomedicine, Trieste, Italy, for providing full access to MFP3D Asylum Research AFM instrumentation. The authors thank Jacob Piehler for supporting us with NTA-EG_3-C_{16}-SH thiol. C.G. acknowledges financial support through the Cluster of Excellence for Macromolecular Complexes (CEF-MC). The authors are happy to acknowledge Federico Benetti for helpful discussion. G.S. would like to dedicate this first of a series of papers on neurodegenerative diseases to the memory of Barbara Yealland of Toronto, who, a few weeks ago lost her battle with ALS but won our hearts for the force, humor, and almost happiness with which she conducted her fight. She will remain as an example of dignity and courage in front of death to the people who have been fortunate enough to know her.

Supporting Information Available: Additional tables and figures concerning nonspecific binding and recMoPrP(89-230) covalent immobilization. This material is available free of charge *via* the Internet at http://pubs.acs.org.

REFERENCES AND NOTES

1. Wingren, C.; Borrebaeck, C. A. K. Progress in Miniaturization of Protein Arrays—A Step Closer to High-Density Nanoarrays. *Drug. Discovery Today* **2007**, *12*, 813–819.
2. Ling, M.; Ricks, C.; Lea, P. Multiplexing Molecular Diagnostics and Immunoassays Using Emerging Microarray Technologies. *Expert Rev. Mol. Diagn.* **2007**, *7*, 87–98.
3. Kusnezow, W.; Syagailo, Y. V.; Goychuk, I.; Hoheisel, J. D.; Wild, D. G. Antibody Microarrays: The Crucial Impact of Mass Transport on Assay Kinetics and Sensitivity. *Expert Rev. Mol. Diagn.* **2006**, *6*, 111–124.
4. Fredriksson, S.; Gullberg, M.; Jarvius, J.; Olsson, C.; Pietras, K.; Gústafsdóttir, S.; Östman, A.; Landegren, U. Protein Detection Using Proximity-Dependent DNA Ligation Assays. *Nat. Biotechnol.* **2006**, *20*, 473–477.
5. Rissin, D. M.; Kan, C. W.; Campbell, T. G.; Howes, S. C.; Fournier, D. R.; Song, L.; Piech, T.; Patel, P. P.; Chang, L.; Rivnak, A. J.; *et al.* Single-Molecule Enzyme-Linked Immunosorbent Assay Detects Serum Proteins at Subfemtomolar Concentrations. *Nat. Biotechnol.* **2010**, *28*, 595–599.
6. Sheehan, P. E.; Whitman, L. J. Detection Limits for Nanoscale Biosensors. *Nano Lett.* **2005**, *5*, 803–807.
7. Lee, K. B.; Park, S. J.; Mirkin, C. A.; Smith, J. C.; Mrksich, M. Protein Nanoarrays Generated by Dip-Pen Nanolithography. *Science* **2002**, *295*, 1702–1705.
8. Tinazli, A.; Piehler, J.; Beuttler, M.; Guckenberger, R.; Tampé, R. Native Protein Nanolithography that Can Write, Read, and Erase. *Nat. Nanotechnol.* **2007**, *2*, 220–225.
9. Artelsmair, H.; Kienberger, F.; Tinazli, A.; Schlapak, R.; Zhu, R.; Preiner, J.; Wruss, J.; Kastner, M.; Saucedo Zeni, N.; Hoelzl, M.; *et al.* Atomic Force Microscopy Derived Nanoscale Chip for the Detection of Human Pathogenic Viruses. *Small* **2008**, *4*, 847–854.
10. Xu, S.; Liu, G. Y. Nanometer-Scale Fabrication by Simultaneous Nanoshaving and Molecular Self-Assembly. *Langmuir* **1997**, *13*, 127–129.
11. Tan, Y. H.; Liu, M.; Nolting, B.; Go, J. G.; Gervay-Hague, J.; Liu, G. Y. A Nanoengineering Approach for Investigation and Regulation of Protein Immobilization. *ACS Nano* **2008**, *2*, 2374–2384.
12. Camarero, J. Recent Developments in the Site-Specific Immobilization of Proteins onto Solid Supports. *Pept. Sci.* **2008**, *90*, 450–458.
13. Polano, M.; Bek, A.; Benetti, F.; Lazzarino, M.; Legname, G. Structural Insights into Alternate Aggregated Prion Protein Forms. *J. Mol. Biol.* **2009**, *393*, 1033–1042.
14. Adamcik, J.; Jung, J.; Flakowski, J.; De Los Rios, P.; Dietler, G.; Mezzenga, R. Understanding Amyloid Aggregation by Statistical Analysis of Atomic Force Microscopy Images. *Nat. Nanotechnol.* **2010**, *5*, 423–428.
15. Cohen, F. E.; Prusiner, S. B. Pathologic Conformations of Prion Proteins. *Annu. Rev. Biochem.* **1998**, *67*, 793–819.

16. Prusiner, S. Prions. *Proc. Natl. Acad. Sci. U.S.A.* **1998**, *95*, 13363–13383.
17. Riek, R.; Hornemann, S.; Wider, G.; Glockshuber, R.; Wüthrich, K. NMR Characterization of the Full-Length Recombinant Murine Prion Protein, mPrp(23-231). *FEBS Lett.* **1997**, *413*, 282–288.
18. Kanaani, J.; Prusiner, S. B.; Diacovo, J.; Baekkeskov, S.; Legname, G. Recombinant Prion Protein Induces Rapid Polarization and Development of Synapses in Embryonic Rat Hippocampal Neurons *in Vitro*. *J. Neurochem.* **2005**, *95*, 1373–1386.
19. Legname, G.; Baskakov, I. V.; Nguyen, H. O.; Riesner, D.; Cohen, F. E.; DeArmond, S. J.; Prusiner, S. B. Synthetic Mammalian Prions. *Science* **2004**, *305*, 673–676.
20. Brown, P.; Cervenáková, L.; Diringer, H. Blood Infectivity and the Prospects for a Diagnostic Screening Test in Creutzfeldt−Jakob Disease. *J. Lab. Clin. Med.* **2001**, *137*, 5–13.
21. Zerr, I.; Kallenberg, K.; Summers, D. M.; Romero, C.; Taratuto, A.; Heinemann, U.; Breithaupt, M.; Varges, D.; Meissner, B.; Ladogana, A.; *et al*. Updated Clinical Diagnostic Criteria for Sporadic Creutzfeldt−Jakob Disease. *Brain* **2009**, *132*, 2659–2668.
22. Huzarewich, R. L.; Siemens, C. G.; Booth, S. A. Application of "Omics" to Prion Biomarker Discovery. *J. Biomed. Biotechnol.* **2010**, *2010*, 613504.
23. Mirmomtaz, E.; Castronovo, M.; Grunwald, C.; Bano, F.; Scaini, D; Ensafi, A. A.; Scoles, G.; Casalis, L. Quantitative Study of the Effect of Coverage on the Hybridization Efficiency of Surface-Bound DNA Nanostructures. *Nano Lett.* **2008**, *8*, 4134–4139.
24. Castronovo, M.; Radovic, S.; Grunwald, C.; Casalis, L.; Morgante, M.; Scoles, G. Control of Steric Hindrance on Restriction Enzyme Reactions with Surface-Bound DNA Nanostructures. *Nano Lett.* **2008**, *8*, 4140–4145.
25. Staii, C.; Wood, D. W.; Scoles, G. Verification of Biochemical Activity for Proteins Nanografted on Gold Surfaces. *J. Am. Chem. Soc.* **2008**, *130*, 640–646.
26. Staii, C.; Wood, D. W.; Scoles, G. Ligand-Induced Structural Changes in Maltose Binding Proteins Measured by Atomic Force Microscopy. *Nano Lett.* **2008**, *8*, 2503–2509.
27. Bano, F.; Fruk, L.; Sanavio, B.; Glettenberg, M.; Casalis, L.; Niemeyer, C. M.; Scoles, G. Toward Multiprotein Nanoarrays Using Nanografting and DNA Directed Immobilization of Proteins. *Nano Lett.* **2009**, *9*, 2614–2618.
28. Ostuni, E.; Chapman, R.; Holmlin, R.; Takayama, S.; Whitesides, G. A Survey of Structure−Property Relationships of Surfaces that Resist the Adsorption of Protein. *Langmuir* **2001**, *17*, 5605–5620.
29. Hochuli, E.; Döbeli, H.; Schacher, A. New Metal Chelate Adsorbent Selective for Proteins and Peptides Containing Neighbouring Histidine Residues. *J. Chromatogr.* **1987**, *411*, 177–184.
30. Sigal, G. B.; Bamdad, C.; Barberis, A.; Strominger, J.; Whitesides, G. M. A Self-Assembled Monolayer for the Binding and Study of Histidine-Tagged Proteins by Surface Plasmon Resonance. *Anal. Chem.* **1996**, *68*, 490–497.
31. Safar, J. G.; Scott, M.; Monaghan, J.; Deering, C.; Didorenko, S.; Vergara, J.; Ball, H.; Legname, G.; Leclerc, E.; Solforosi, L.; *et al*. Measuring Prions Causing Bovine Spongiform Encephalopathy or Chronic Wasting Disease by Immunoassays and Transgenic Mice. *Nat. Biotechnol.* **2002**, *20*, 1147–1150.
32. Williamson, R. A.; Peretz, D.; Pinilla, C.; Ball, H.; Bastidas, R. B.; Rozenshteyn, R.; Houghten, R. A.; Prusiner, S. B.; Burton, D. R. Mapping the Prion Protein Using Recombinant Antibodies. *J. Virol.* **1998**, *72*, 9413–9418.
33. Luginbühl, B.; Kanyo, Z.; Jones, R.; Fletterick, R.; Prusiner, S.; Cohen, F.; Williamson, R.; Burton, D.; Plückthun, A. Directed Evolution of an Anti-prion Protein scFv Fragment to an Affinity of 1 pM and Its Structural Interpretation. *J. Mol. Biol.* **2006**, *363*, 75–97.
34. Zahn, R.; Liu, A.; Lührs, T.; Riek, R.; von Schroetter, C.; López García, F.; Billeter, M.; Calzolai, L.; Wider, G.; Wüthrich, K. NMR Solution Structure of the Human Prion Protein. *Proc. Natl. Acad. Sci. U.S.A.* **2000**, *97*, 145–150.
35. *CRC Handbook of Chemistry and Physics,* 90th ed.; Lide, D. R., Ed.; CRC Press, Taylor and Francis: New York, 2009.
36. Valiokas, R.; Klenkar, G.; Tinazli, A.; Reichel, A.; Tampé, R.; Piehler, J.; Liedberg, B. Self-Assembled Monolayers Containing Terminal Mono-, Bis-, and Tris-Nitrilotriacetic Acid Groups: Characterization and Application. *Langmuir* **2008**, *24*, 4959–4967.
37. Riek, R; Hornemann, S; Wider, G; Billeter, M; Glockshuber, R; Wüthrich, K. NMR Structure of the Mouse Prion Protein Domain PrP(121-231). *Nature* **1996**, *382*, 180–182.
38. Calzolai, L.; Zahn, R. Influence of pH on NMR Structure and Stability of the Human Prion Protein Globular Domain. *J. Biol. Chem.* **2003**, *278*, 35592–35596.
39. Yang, T.; Baryshnikova, O. K.; Mao, H.; Holden, M. A.; Cremer, P. S. Investigations of Bivalent Antibody Binding on Fluid-Supported Phospholipid Membranes: The Effect of Hapten Density. *J. Am. Chem. Soc.* **2003**, *125*, 4779–4784.
40. Schwarz, G.; Stankowski, S. Linear cooperative binding of large ligands involving mutual exclusion of different binding modes. *Biophys. Chem.* **1979**, *10*, 173–181.
41. Kruppa, M.; Konig, B. Reversible Coordinative Bonds in Molecular Recognition. *Chem. Rev.* **2006**, *106*, 3520–3560.
42. Saborio, G. P.; Permanne, B.; Soto, C. Sensitive Detection of Pathological Prion Protein by Cyclic Amplification of Protein Misfolding. *Nature* **2001**, *411*, 810–813.
43. Kranjc, A.; Bongarzone, S.; Rossetti, G.; Biarnés, X.; Cavalli, A.; Bolognesi, M. L.; Roberti, M.; Legname, G.; Carloni, P. Docking Ligands on Protein Surfaces: The Case Study of Prion Protein. *J. Chem. Theory Comput.* **2009**, *5*, 2565–2573.
44. Vendruscolo, M.; Zurdo, J.; MacPhee, C. E.; Dobson, C. M. Protein Folding and Misfolding: A Paradigm of Self-Assembly and Regulation in Complex Biological Systems. *Philos. Trans. A* **2003**, *361*, 1205–1222.
45. Gupta, P.; Loos, K.; Korniakov, A.; Spagnoli, C.; Cowman, M.; Ulman, A. Facile Route to Ultraflat SAM-Protected Gold Surfaces by "Amphiphile Splitting". *Angew. Chem., Int. Ed.* **2004**, *43*, 520–523.
46. Ulman, A. Formation and Structure of Self-Assembled Monolayers. *Chem. Rev.* **1996**, *96*, 1533–1554.
47. Hegner, M.; Wagner, P.; Semenza, G. Ultralarge Atomically Flat Template-Stripped Au Surfaces for Scanning Probe Microscopy. *Surf. Sci.* **1993**, *291*, 36–46.
48. Go, J.; Alam, M. Statistical Interpretation of "Femtomolar" Detection. *Appl. Phys. Lett.* **2009**, *95*, 033110.